Numerical Solution to Drop Coalescence/Breakup with a Volume-Conserving, Positive-Definite, and Unconditionally Stable Scheme

M. Z. JACOBSON

Department of Civil and Environmental Engineering, Stanford University, Stanford, California

(Manuscript received 8 July 2010, in final form 22 October 2010)

ABSTRACT

This paper discusses a new volume- and volume concentration–conserving, positive-definite, unconditionally stable iterative numerical scheme for solving temporary cloud/raindrop coalescence followed by breakup and the coupling of the scheme with an existing noniterative, volume- and volume concentration–conserving collision/coalescence (coagulation) scheme. The breakup scheme alone compares nearly exactly with a constant-kernel analytical solution at a 300-s time step. The combined coagulation/breakup schemes are stable and conservative, regardless of the time step and number of size bins, and convergent with higher temporal and size resolution. The schemes were designed with these characteristics in mind for use in long-term global or regional simulations. The use of 30 geometrically spaced size bins and a time step of 60 s provides a good compromise between obtaining sufficient accuracy (relative to a much higher-resolution result) and speed, although solutions with a 600-s time step and 30 bins are stable and conservative and take one-eighth the computer time. The combined coagulation/breakup schemes were implemented into the nested Gas, Aerosol, Transport, Radiation, General Circulation, Mesoscale, and Ocean Model (GATOR-GCMOM), a global–urban climate–weather–air pollution model. Coagulation was solved over liquid, ice, and graupel distributions and breakup simultaneously over the liquid distribution. Each distribution included 30 size bins and 16 chemical components per bin. Timing tests demonstrate the feasibility of the scheme in long-term global simulations.

1. Introduction

The solution to the integro-differential equation for the combined processes of cloud drop collision/coalescence (coagulation) and collision/temporary coalescence/breakup (breakup) is a challenging numerical problem for which few satisfying solutions have been developed. The purpose of this paper is to present a new volume- and volume concentration (that is, volume multiplied by number concentration)–conserving, positive-definite, iterative numerical solution to the breakup component of this equation and a method of coupling the scheme with an existing volume- and volume concentration–conserving noniterative coagulation scheme.

The integro-differential equation for coagulation and breakup is

$$\frac{\partial n_v}{\partial t} = \frac{1}{2}\int_0^v \beta_{v-\bar{v},\bar{v}} n_{v-\bar{v}} n_{\bar{v}}\, d\bar{v} - n_v \int_0^\infty \beta_{v,\bar{v}} n_{\bar{v}}\, d\bar{v} + \frac{1}{2}\int_0^\infty \int_0^\infty B_{v',v''} P_{v;v',v''} n_{v'} n_{v''}\, dv'\, dv'' - n_v \int_0^\infty B_{v,\bar{v}} n_{\bar{v}}\, d\bar{v}, \quad (1)$$

where n is the time-dependent particle number concentration (particles per cubic centimeter of air); $v - \bar{v}$ and $\bar{v}$ are the single-particle volumes of two colliding/coalescing particles; v is the volume of the new, permanently coalesced particle; β is the coagulation kernel (rate coefficient; cubic centimeters per particle per second) of colliding particle pair $v - \bar{v}$, $\bar{v}$ or v, $\bar{v}$; B is the breakup kernel (cubic centimeters per particle per second) for particle pair v', v''; and P is the number of fragments of volume v per temporarily coalescing colliding pair v', v''. The coagulation portion of Eq. (1) (first two terms) is applied to aerosol and hydrometeor size distributions. The breakup portion (last two terms) is applied generally to hydrometeor particles.

Corresponding author address: M. Z. Jacobson, Dept. of Civil and Environmental Engineering, Y2E2 Building, 473 Via Ortega, Room 397, Stanford University, Stanford, CA 94305–4020.
E-mail: jacobson@stanford.edu

DOI: 10.1175/2010JAS3605.1

Many solutions exist to the coagulation portion of Eq. (1). Some solutions for aerosol particles have assumed that particles are spread over lognormal modes (e.g., Pratsinis 1988; Binkowski and Shankar 1995). Other solutions for aerosols have assumed discrete aerosol size distributions (e.g., Gelbard and Seinfeld 1978; Suck and Brock 1979; Strom et al. 1992; Jacobson et al. 1994; Fassi-Fihri et al. 1997; Trautmann and Wanner 1999; Fernandez-Diaz et al. 2000; Sandu 2002; Jacobson 2002). Solutions for hydrometeor particles over discrete size distributions have also been developed (e.g., Bleck 1970; Tzivion et al. 1987; Hounslow et al. 1988; Lister et al. 1995; Bott 2000; Jacobson 2003). The discretized solutions generally conserve various properties, but almost all are explicit, thereby requiring a time step limited by stability constraints. Furthermore, almost all numerical solutions have treated coagulation over only one size distribution. Jacobson et al. (1994) and Jacobson (2002, 2003) developed noniterative, semi-implicit, volume conserving, and volume concentration–conserving coagulation schemes for any number of discrete aerosol and/or hydrometeor distributions, any number of size bins per distribution, and any number of components per size bin that were unconditionally stable for any time step. These solutions also converged to exact solutions with higher size bin resolution.

With respect to breakup, Hu and Srivastava (1995), Brown (1997, 1999), and Seifert et al. (2005, hereafter S05) applied the coagulation scheme of Bleck (1970), extended to breakup, operator-splitting the solution from that of coagulation. Gillespie and List (1978) and List et al. (1987) similarly extended the finite-element coagulation solution of Gelbard and Seinfeld (1978) to include breakup. That scheme has also been used by McFarquhar (2004) and others. Feingold et al. (1988) extended the method-of-moments coagulation scheme of Tzivion et al. (1987) to drop breakup using a transformation from Bleck (1970).

All extended schemes appear to work well, but all are explicit and thus subject to a limit on the time step based on stability and positive-definiteness constraints. This is not so much of an issue for box or 3D cloud models run for hours to days, but for 3D global or regional climate models that may be run for years or decades, it is desirable to have the flexibility of using any time step without the possibility of a negative number or an otherwise unstable solution, while conserving volume exactly (which coagulation and breakup physically do). Although coarsely-resolved-in-space models have significant uncertainty with respect to predicting cloud properties, some such models, including the model applied here, treat cumulus clouds as subgrid phenomena and cloud microphysical processes in some detail. The present parameterization may be particularly beneficial for such models as it increases the detail of breakup numerics to a level similar to that of other microphysical processes. Below, such a scheme is presented. First, the size grid used here and some of the major terms in Eq. (1) are discussed.

2. Size grid, kernels, and coalescence efficiencies

The numerical solutions discussed here can be obtained with any discretized size distribution. However, here, Eq. (1) is discretized over $i = 1, \ldots, N_C$ geometrically spaced hydrometeor size bins between low and high diameters of 0.5 μm–8 mm. In this distribution, the single-particle volume (cm^3) in size bin $i + 1$ equals that in bin i multiplied by a constant, V_{rat}: $v_{i+1} = V_{rat} v_i$. For a given low and high central volume (or diameter d) of the bin and a specified number of size bins,

$$V_{rat} = \left(\frac{v_{N_C}}{v_1}\right)^{1/(N_C-1)} = \left(\frac{d_{N_C}}{d_1}\right)^{3/(N_C-1)}. \quad (2)$$

Subsequent equations will be written in terms of a discretized size distribution.

a. Coagulation and breakup kernels and coalescence efficiencies

The discretized form of the coagulation kernel for particles of size i and j (cubic centimeters per particle per second) is

$$\beta_{i,j} = K_{i,j} E_{coal,i,j}, \quad (3)$$

where $K_{i,j}$ is a collision kernel (cubic centimeters per particle per second) and $E_{coal,i,j}$ is a coalescence efficiency (dimensionless). The total collision kernel for aerosol and hydrometeor particles accounts for the kernels due to Brownian motion, Brownian diffusion enhancement, van der Waal's forces, viscous forces, fractal geometry, gravitational collection, turbulent shear, turbulent inertial motion, diffusiophoresis, thermophoresis, and electric charge (Jacobson 2003, 2005). For gravitational collection alone, used here for some tests, the kernel is

$$K_{g,i,j} = E_{coll,i,j} \pi (r_i + r_j)^2 |V_{f,i} - V_{f,j}|, \quad (4)$$

where $E_{coll,i,j}$ is a dimensionless collision efficiency [taken from Beard and Grover (1974)], r is drop radius (cm), and V_f is the terminal fall speed (cm s^{-1}), calculated here from the parameterization of Beard (1976), as given in Jacobson [2005, his Eq. (20.9)].

When particles collide but do not permanently coalesce, they temporarily coalesce and then break up. The breakup kernel (cubic centimeters per particle per second) is

$$B_{i,j} = K_{i,j}(1 - E_{\text{coal},i,j}) = \beta_{i,j}(1 - E_{\text{coal},i,j})/E_{\text{coal},i,j}, \quad (5)$$

where $E_{\text{coal},i,j}$ is a dimensionless coalescence efficiency.

Coalescence efficiencies used here are obtained from Beard and Ochs (1995, hereafter BO95) for small-particle diameter $d_s < 300$ μm, from Low and List (1982a, hereafter LL82a) for $d_s > 500$ μm, and from an interpolation formula between the two ranges from S05.

BO95 give efficiencies in two ranges: d_s from 14 to 200 μm and d_s from 200 to 800 μm. For $d_s < 14$ μm, the efficiencies converge to 1. For the smaller range (14–200 μm), the coalescence efficiency is found by a Newton–Raphson iteration (with iteration number n) with

$$E_{c,f,i,j,n+1} = \frac{A_0 + E_{c,f,i,j,n}[A_1 + E_{c,f,i,j,n}(A_2 + E_{c,f,i,j,n}A_3)] - \ln[r_s(\mu\text{m})] - \ln[r_b(\mu\text{m})/200]}{A_1 + E_{c,f,i,j,n}(2A_2 + 3E_{c,f,i,j,n}A_3)}, \quad (6)$$

where $A_0 = 5.07$, $A_1 = -5.94$, $A_2 = 7.27$, and $A_3 = -5.29$; r_s is the small-particle radius (μm); and r_b is the big-particle radius (μm). This equation converges within four iterations with a first guess of $E_{c,f,i,j,1} = 0.5$. For the larger range (200–800 μm), the BO95 coalescence efficiency is

$$E_{c,e,i,j} = \max\left[0.767 - 10.14\frac{2^{1.5}}{6\pi}\frac{q^4(1+q)\sqrt{\text{We}^*_{i,j}}}{(1+q^2)(1+q^3)}, 0\right], \quad (7)$$

where $q = r_s/r_b$ and

$$\text{We}^*_{i,j} = \rho_w r_s (V_{f,b} - V_{f,s})^2/\sigma_w \quad (8)$$

is the Weber number (dimensionless) for engineering and fluid dynamics applications. In this equation, ρ_w is liquid water density (g cm^{-3}), ρ_w is liquid water surface tension (dyn cm^{-1} = g s^{-2}), and V_f is the fall speed of the big and small drops (cm s^{-1}). The overall BO95 coalescence efficiency is then taken as (S05)

$$E_{c,\text{bo},i,j} = \min[\max(E_{c,e,i,j}, E_{c,f,i,j}), 1]. \quad (9)$$

The LL82a parameterization for coalescence efficiency at large particle diameter is

$$E_{c,\text{ll},i,j} = a\left(1 + \frac{d_s}{d_b}\right)^{-2} \exp\left(-\frac{b\sigma_w E^2_{T,i,j}}{S_{c,i,j}}\right) \quad \text{for} \quad E_{T,i,j} < 5.0 \times 10^{-6}\ \text{J} \quad (10)$$

(otherwise, zero), where $a = 0.778$, $b = 2.61 \times 10^6$ m^2 J^{-2}, σ_w here is in units of Joules per square centimeter, and d_s and d_b are the small- and big-particle diameters (cm), respectively. In addition,

$$E_{T,i,j} = \text{CKE}_{i,j} + \Delta S_{i,j} \quad (11)$$

is the total coalescence energy (J) of the two colliding drops,

$$\text{CKE}_{i,j} = \frac{\pi\rho_w}{12}\frac{d_b^3 d_s^3}{(d_b^3 + d_s^3)}(V_{f,b} - V_{f,s})^2 \quad (12)$$

is the collision kinetic energy of the colliding drops (J),

$$S_{T,i,j} = \pi\sigma_w(d_b^2 + d_s^2) \quad (13)$$

is the summed surface energies (J) of the two drops before collision (with σ_w in Joules per square centimeter),

$$S_{c,i,j} = \pi\sigma(d_b^3 + d_s^3)^{2/3} \quad (14)$$

is the surface energy (J) of the spherical equivalent of the coalesced drop, and

$$\Delta S_{i,j} = S_{T,i,j} - S_{c,i,j} \quad (15)$$

is the difference between the total surface energy (J) of the two individual drops on their own and the surface energy of the single spherical temporarily coalesced drop.

The interpolation formula between the BO95 and LL82a efficiencies, modified slightly for the range of application from S05, is

$$E_{c,i,j} = \begin{cases} E_{c,\text{bo},i,j}, & d_s < 300\,\mu\text{m} \\ \cos^2\left[\frac{\pi}{2}\frac{(d_s - 300\,\mu\text{m})}{200\,\mu\text{m}}\right]E_{c,\text{bo},i,j} + \sin^2\left[\frac{\pi}{2}\frac{(d_s - 300\,\mu\text{m})}{200\,\mu\text{m}}\right]E_{c,\text{ll},i,j} & \\ E_{c,\text{ll},i,j}, & d_s > 500\,\mu\text{m} \end{cases}. \quad (16)$$

Figure 1 shows coalescence efficiencies from Eq. (16) under near-surface conditions, with which the experiments resulting in the underlying parameterizations were performed. The figure follows Fig. 3 of S05 closely despite the slight difference in the range of interpolation. The figure here is also extended to slightly higher diameter.

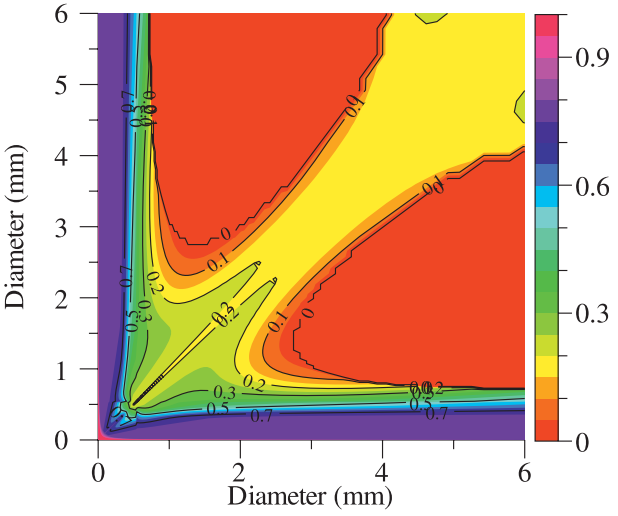

FIG. 1. Coalescence efficiencies determined from Eq. (16), which relies on efficiencies from BO95 for $d_s < 0.3$ mm, from LL82a for $d_s > 0.5$ mm, and an interpolation formula from S05 between the two. Efficiencies were obtained at a temperature of 20°C and pressure of 1013 hPa.

b. Breakup distribution

The solution to drop breakup requires the specification of a breakup distribution for each colliding pair of drops. Here, we use the formulation from Straub et al. (2010, hereafter S10), who based their parameterization on a matrix of 32 drop pairs with small and large diameters ranging from 0.02 to 0.5 cm, including 10 pairs considered from Low and List (1982b). Although this parameterization is based on small drops down to 0.02 cm only, Brown (1999, see his Fig. 3) suggests that drops much smaller than this colliding with large drops can result in breakup. As such, we somewhat arbitrarily apply the S10 parameterization down to 0.005-cm diameter. Below this diameter, we assume that noncoalescing collision [as determined by one minus Eq. (16)] results in bounceoff, but not breakup.

The S10 parameterization involves determining the number of fragments in model size bin l per temporarily coalescing pair i, j as

$$P_{i,j,l} = p_{i,j,l,1} + p_{i,j,l,2} + p_{i,j,l,3} + p_{i,j,l,4}, \tag{17}$$

where the ps are the number of fragments in size l per temporarily coalescing pair i, j from each of four breakup size distribution ranges. The size distribution in range 1 is a lognormal distribution with

$$p_{i,j,l,1} = \frac{N_1 \Delta d_l}{d_l \sigma_{g,1} \sqrt{2\pi}} \exp\left[-\frac{(\ln d_l - \mu_1)^2}{2\sigma_{g,1}^2}\right], \tag{18}$$

where

$$N_1 = \max\left[0.088\left(\frac{d_b}{d_s}\mathrm{CW}_{i,j} - 7\right), 0\right] \tag{19}$$

is the number of fragments summed over the entire lognormal distribution per temporarily coalescing pair,

$$\mu_1 = \ln D_1 - \frac{\sigma_{g,1}^2}{2} \tag{20}$$

is the geometric mean number diameter (cm) of the distribution,

$$\sigma_{g,1}^2 = \ln\left(\frac{\mathrm{Var}}{D_1^2} + 1\right) \tag{21}$$

is the square of the geometric standard deviation, $\mathrm{Var} = (0.0125)^2 \mathrm{CW}_{i,j}/12$ is the variance, and $D_1 = 0.04$ cm. In these equations, $\mathrm{CW}_{i,j} = (\mathrm{CKE}_{i,j})(\mathrm{We}_{i,j})$, where $\mathrm{We}_{i,j} = \mathrm{CKE}_{i,j}/S_{c,i,j}$ is another form of the dimensionless Weber number.

The size distributions in ranges 2 and 3 are normal distributions. For range 2, the number of fragments in size l per temporarily coalescing pair i, j is

$$p_{i,j,l,2} = \frac{N_2 \Delta d_l}{\sigma_2 \sqrt{2\pi}} \exp\left[-\frac{(d_l - D_2)^2}{2\sigma_2^2}\right], \tag{22}$$

where the number of fragments per colliding pair, summed over the distribution, is

$$N_2 = \max[0.22(\mathrm{CW}_{i,j} - 21), 0] \tag{23}$$

and the normal-distribution mean number diameter is $D_2 = 0.095$ cm. The normal-distribution standard deviation is

$$\sigma_2 = \frac{\max[0.007(\mathrm{CW}_{i,j} - 21), 0]}{\sqrt{12}}. \tag{24}$$

For range 3, the number of fragments in size l per temporarily coalescing pair i, j is

$$p_{i,j,l,3} = \frac{N_3 \Delta d_l}{\sigma_3 \sqrt{2\pi}} \exp\left[-\frac{(d_l - D_3)^2}{2\sigma_3^2}\right], \tag{25}$$

TABLE 1. Number of drop fragments N_T per colliding pair for laboratory-based and high-resolution computation-based drop pair determinations given in S10 (see their Table 1). Results were obtained at a temperature of 20°C and pressure of 1013 hPa. Other conditions, including CKE, were obtained from Table 1 of Schlottke et al. (2010).

Pair	d_s (cm)	d_b (cm)	N_T (S10)	N_T (here)	Pair	d_s (cm)	d_b (cm)	N_T (S10)	N_T (here)
1	0.0395	0.18	2	2	17	0.0395	0.32	2	2
2	0.0395	0.40	2	2	18	0.14	0.41	7.83	7.8
3	0.0395	0.44	2	2	19	0.06	0.24	2	2
4	0.0715	0.18	2	2	20	0.07	0.3	2.45	2.45
5	0.1	0.18	2	2	21	0.07	0.36	2.72	2.72
6	0.1	0.18	3.58	3.57	22	0.07	0.45	2.81	2.81
7	0.1	0.30	4.52	4.52	23	0.1	0.12	2	2
8	0.1	0.46	5.02	5.01	24	0.1	0.41	4.93	4.92
9	0.18	0.36	5.73	5.7	25	0.12	0.25	2.56	2.56
10	0.18	0.46	10.24	10.2	26	0.12	0.3	3.99	3.98
11	0.035	0.06	2	2	27	0.12	0.36	5.56	5.55
12	0.035	0.12	2	2	28	0.12	0.46	6.6	6.58
13	0.06	0.12	2	2	29	0.14	0.36	6.2	6.17
14	0.0395	0.25	2	2	30	0.16	0.18	2	2
15	0.09	0.24	2.35	2.34	31	0.16	0.41	9.05	9.02
16	0.15	0.27	2.7	2.7	32	0.18	0.25	2	2

where the number of fragments per pair, summed over the distribution, is

$$N_3 = \max\{\min[0.04(46 - \mathrm{CW}_{i,j}), 1]0\}, \quad (26)$$

the normal-distribution mean number diameter is $D_3 = 0.9d_s$ cm, and the standard deviation is

$$\sigma_3 = \frac{0.01(1 + 0.76\sqrt{\mathrm{CW}_{i,j}})}{\sqrt{12}}. \quad (27)$$

For each range $k = 1$–3, the sum of $p_{i,j,l,k}$ over all discrete sizes $l = 1, \ldots, N_C$ converges to N_k with increasing size resolution (smaller values of V_{rat}). However, for coarse size resolution, the sum is less than N_k. To ensure exact number conservation, $p_{i,j,l,k}$ is normalized here with

$$p_{i,j,l,k} = p_{i,j,l,k} \frac{N_k}{\sum_{l=1}^{N_C} p_{i,j,l,k}} \quad (28)$$

after $p_{i,j,l,k}$ is first solved.

Finally, for range 4, the number of fragments per temporarily coalescing pair is determined by conserving volume between the volumes of the original coalescing pair and the summed volumes among all fragments of all sizes. The exact volumes (cm^3) of fragments, summed over all sizes for each range 1–3, respectively, are (S10)

$$V_{b,1} = \frac{\pi}{6} N_1 \exp\left(3\mu_1 + \frac{9}{2}\sigma_{g,1}^2\right), \quad (29)$$

$$V_{b,2} = \frac{\pi}{6} N_2 \exp(\mu_2^3 + 3\mu_2\sigma_2^2), \quad (30)$$

$$V_{b,3} = \frac{\pi}{6} N_3 \exp(\mu_3^3 + 3\mu_3\sigma_3^2). \quad (31)$$

To conserve volume, one more single fragment is produced from the volume-conservation relationship:

$$V_{b,4} = \frac{\pi}{6}(d_i^3 + d_j^3) - V_{b,1} - V_{b,2} - V_{b,3}. \quad (32)$$

However, since the single fragment in range 4 does not fall exactly into a discrete model size bin, its volume and number must be partitioned here between two adjacent discrete bins whose centers surround $v_{b,4}$ in a number- and volume-conserving manner. The resulting number concentrations partitioned to adjacent bins l and $l + 1$ are determined for the present size bin structure as

$$n_l = \frac{v_{l+1} - V_{b,4}}{v_{l+1} - v_l} \quad \text{and} \quad (33)$$

$$n_{l+1} = 1 - n_l, \quad (34)$$

respectively. In sum, the total number of fragments produced per colliding pair is

$$N_{T,i,j} = N_1 + N_2 + N_3 + 1 \quad (35)$$

and the total volume of such fragments is $V_{b,1} + V_{b,2} + V_{b,3} + V_{b,4} = \pi(d_i^3 + d_j^3)/6$; thus, the volume of the breakup distribution for each colliding pair is conserved exactly.

Table 1 compares the number of fragments calculated from Eq. (35) here with those calculated by S10 (see their Table 1) for 32 colliding pairs of drops for which laboratory or high-resolution model data were available. The calculations here give almost identical results to

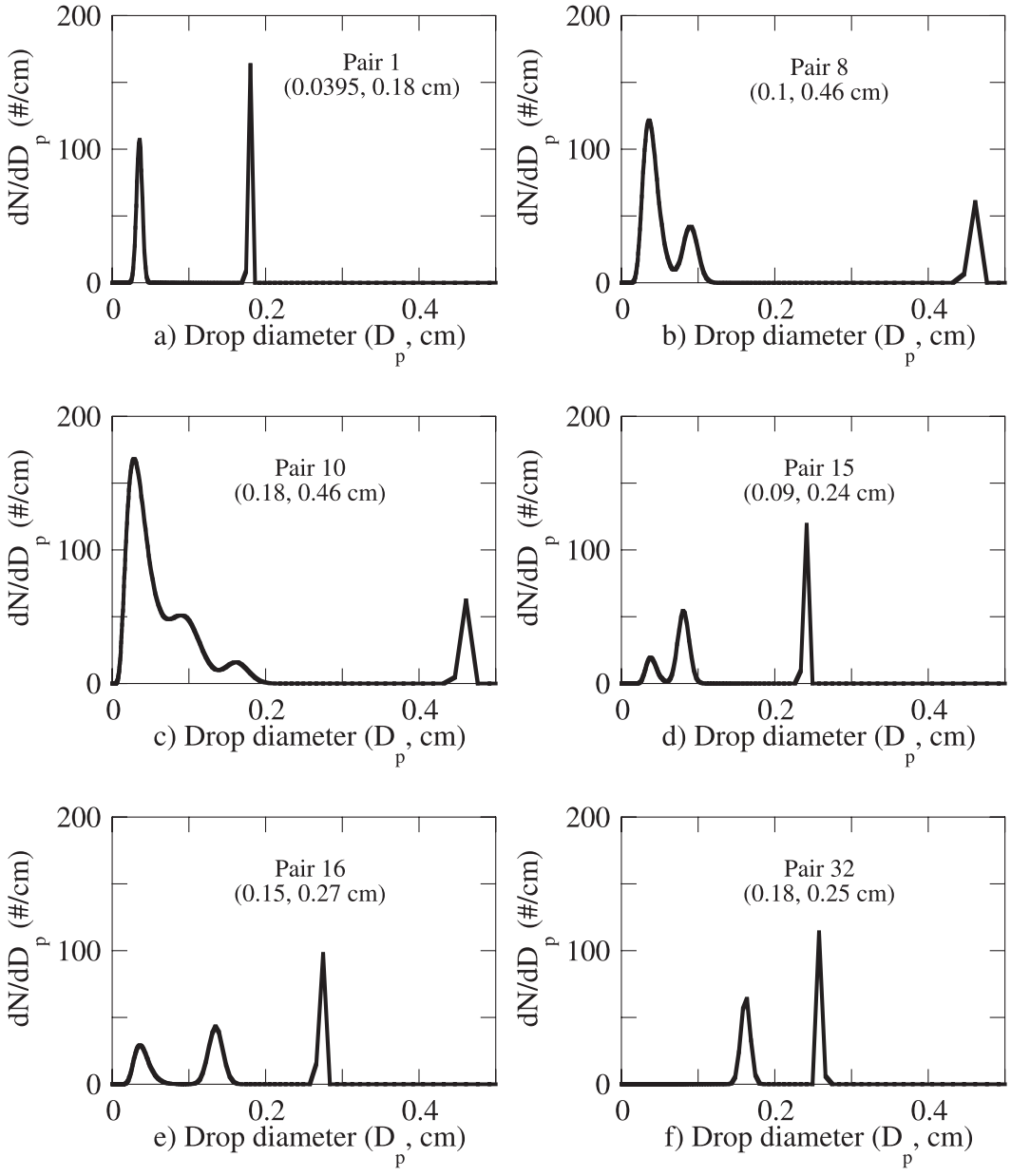

FIG. 2. Breakup size distributions of six colliding drop pairs with the method of S10 calculated over 300 discrete size bins from 0.5 μm to 8 mm in diameter. The figures can be compared with the corresponding pairs in Fig. 5 of S10. The numbers below the pair identifier are the small- and big-particle diameters resulting in the temporarily coalesced pair that breaks up.

those in S10. Figure 2 shows the calculated size distributions of six of these pairs over 300 discretized size bins from 0.5 μm to 8 mm, which also compare well with results shown in Fig. 5 of S10.

Figure 3 shows the number of fragments per colliding drop pair from Eq. (35) for the entire size distribution of colliding particles up to 6 mm. The figure indicates a peak in the number of breakup fragments when particles of 2 mm collide with those of 5 mm. Minima occur for equal-sized drops and for very large drops colliding with much smaller drops.

c. Solution to collision/coalescence (coagulation)

The numerical solution to Eq. (1) is obtained first by operator-splitting the coagulation and breakup solutions. Previous solutions to Eq. (1) have been operator split as well (section 1). The effect of different operator-splitting time steps will be examined. Below, the coagulation solution

is first shown. A new method of solving for breakup is then given.

The collision/coalescence (coagulation) terms in Eq. (1) are solved with the semi-implicit solution of Jacobson et al. (1994) and Jacobson (2002, 2003). The scheme assumes that particles of each size contain multiple components $q = 1, N_V$, where the sum of the volume concentration of each component in each size bin $v_{q,i}$ (cubic centimeters of particles per cubic centimeters of air) over all components in the size bin equals to the total volume concentration of particles in the bin v_i. Further, the number concentration is related to the total volume concentration and the single-particle volume in the bin by $n_i = v_i/v_i$. The scheme can be applied to any number of aerosol or hydrometeor size distributions simultaneously, as shown in Jacobson (2002, 2003). In fact, for the 3D model application discussed here, it is implemented for liquid, ice, and graupel size distributions simultaneously. However, below the solution is shown for one size distribution for illustrative purposes.

The scheme is noniterative, positive-definite, unconditionally stable, and conservative of single-particle volume and volume concentration for all particle components and the total particle. Number concentration converges to the exact solution upon an increase in resolution. The coagulation solution, in terms of the volume concentration (cubic centimeters per cubic centimeters of air) of component q within particles in aerosol-contrail size bin k at time t after one time step h (s) is

$$v_{q,k,t} = \frac{v_{q,k,t-h} + h\sum_{j=1}^{k}\left(\sum_{i=1}^{k-1} f_{i,j,k}\beta_{i,j}v_{q,i,t}n_{j,t-h}\right)}{1 + h\sum_{j=1}^{N_B}[(1 - f_{k,j,k})\beta_{k,j}n_{j,t-h}]}, \quad (36)$$

where

$$f_{i,j,k} = \begin{cases} \left(\dfrac{v_{k+1} - V_{i,j}}{v_{k+1} - v_k}\right) & v_k \le V_{i,j} < v_{k+1} \quad k < N_B \\ 1 - f_{i,j,k-1} & v_{k-1} \le V_{i,j} < v_k \quad k > 1 \\ 1 & V_{i,j} > v_k \quad k = N_B \\ 0 & \text{all other cases} \end{cases} \quad (37)$$

is the volume fraction of a coagulated pair i, j, with volume single-particle volume $V_{i,j} = v_i + v_j$, partitioned into bin k. This intermediate particle has volume between those of two model bins, k and $k + 1$, and needs to be partitioned between the two.

Equation (36) is solved in the order $k = 1, \ldots, N_C$. No production occurs into the first bin, $k = 1$, since $k - 1 = 0$ for the first bin in the numerator of Eq. (36). Thus, all necessary $v_{q,i,t}$ terms are known when each $v_{q,k,t}$ is calculated. Once the equation is solved, $v_{k,t}$ (cubic centimeters per cubic centimeters of air) is recalculated by summing $v_{q,k,t}$ over all components $q = 1, N_V$ and new number concentrations (particles per cubic centimeter) are $n_{k,t} = v_{k,t}/v_k$.

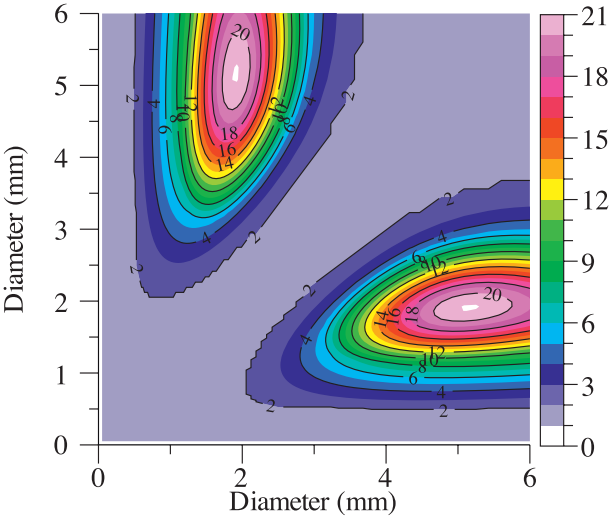

FIG. 3. Number of resulting fragments per colliding drop pair from Eq. (35), which relies on the parameterization of S10. Results were obtained at a temperature of 20°C and pressure of 1013 hPa. Note that the fall speed used to calculate CKE for this figure [as described under Eq. (4)] differs from that used to calculate it in Table 1, so the number of fragments differ slightly.

d. Solution to drop breakup

The numerical solution to drop breakup is determined here as follows. Breakup involves two terms [last two terms in Eq. (1)]: one that gives the production of new fragments in a given size bin and the other that describes the loss of drops to collision/temporary coalescence/breakup. Since drops of each size compete simultaneously with drops of every other size for collision/temporary coalescence, it is necessary to solve for the loss of drops implicitly rather than explicitly, both for accuracy (e.g., faster convergence upon refining the size grid and time step) and stability. The present scheme allows for stability with any time step and size grid resolution although accuracy improves upon increasing both. Concentrations from the implicit solution are then applied to the breakup distribution to determine the number of new fragmented drops in a manner consistent with the loss terms.

The implicit solution to the loss term [fourth term in Eq. (1)] is obtained by first writing the term as

$$\frac{dn_i}{dt} = -n_i\sum_{j=1}^{N_C} B_{i,j}n_j \quad (38)$$

and then discretizing the equation further with

$$n_{i,t} = n_{i,t-h} - h n_{i,t} \sum_{j=1}^{N_C} B_{i,j} n_{j,t}, \tag{39}$$

where h is the time step size (s), t is the current time step, and $t - h$ is the previous time step. This equation can be solved exactly but iteratively for any time step among all size bins $i = 1, \ldots, N_C$ simultaneously with

$$n_{i,t,n+1} = \frac{n_{i,t-h}}{1 + h \sum_{j=1}^{N_C} B_{i,j} n_{j,t,n,\text{est}}}, \tag{40}$$

where the subscript n is the iteration number. For each iteration, it is necessary to solve Eq. (40) for all size bins i before moving on to the next iteration. The estimated value in the denominator of Eq. (40) is determined as

$$n_{i,t,n,\text{est}} = (n_{i,t,n} + n_{i,t,n-1,\text{est}})/2, \tag{41}$$

with $n_{i,t,0,\text{est}} = n_{i,t-h}$ and $n_{i,t,1} = n_{i,t-h}$. The use of an estimated value instead of a value from iteration n in Eq. (40) speeds up convergence significantly by preventing the solution from oscillating between two vastly different numbers on its way to convergence. Convergence is said to occur when

$$\frac{\sum_{j=1}^{N_C} n_{j,t,n+1} - \sum_{j=1}^{N_C} n_{j,t,n}}{\sum_{j=1}^{N_C} n_{j,t,n}} < 10^{-16} \rightarrow \text{convergence}. \tag{42}$$

The advantage of this convergence criterion is that the computational time for it is low, since the division is taken outside of the summation loop (and divisions require ~12 times more computer time than additions), and the accuracy is the same as any other criterion.

For 30–300 size bins, convergence generally occurs within 15–70 iterations. Since only one equation is iterated across all size bins, the computer time for iteration is minimized (computer timings are discussed in section 3). The iteration technique described is related to that developed for the multistep implicit–explicit (MIE) method, used to solve chemical ordinary differential equations (Jacobson and Turco 1994). With the MIE method, the forward Euler and the linearized backward Euler schemes are iterated, both with reaction rates determined from the linearized backward Euler scheme. Convergence of both the forward and linearized backward Euler schemes individually and to each other is guaranteed, as demonstrated in Jacobson [2005, his Eqs. (12.66) and (12.67) and Fig. 12.1], and the resulting solution conserves mass and is positive definite. Since both converge, it is necessary only to solve either the forward Euler or linearized backward Euler schemes so long as the one chosen is converged completely. In the present case, we iterate the linearized backward Euler [Eq. (40), as applied to breakup] until convergence.

Once convergence has occurred, the number concentration (particles per cubic centimeter) of temporarily coalesced drops for each pair $i = 1, N_C$, $j = i, N_C$ is now

$$R_{i,j,t} = \begin{cases} B_{i,j} n_{i,t} n_{j,t} & \text{for} \quad i \neq j \\ 0.5 B_{i,j} n_{i,t} n_{j,t} & \text{for} \quad i = j \end{cases}. \tag{43}$$

The 0.5 is not needed for $i \neq j$ since $R_{i,j,t}$ is evaluated and used only for $j = i, N_C$, not $j = 1, N_C$, so production terms are not double counted. The fragments of the temporarily coalesced pairs are then distributed among each size $l = 1, N_C$ with

$$n_{l,t} = n_{l,t} + R_{i,j,t} P_{i,j,l}, \quad \text{for each } i = 1, N_C \text{ and } j = i, N_C, \tag{44}$$

which results in exact volume conservation. This equation also gives the total number of fragments per temporarily coalesced pair over all sizes exactly as $N_{T,i,j}$ [Eq. (35)].

Next, since each drop contains multiple chemical components, it is necessary to solve for the redistribution of particle components during temporary coalescence/fragmentation. This is accomplished exactly for each $q = 1, N_V$ component with

$$v_{q,i,t} = v_{q,i,t} - \frac{v_{q,i,t-h}}{n_{i,t-h}} R_{i,j,t}, \quad \text{for each } i = 1, N_C; j = i, N_C, \tag{45}$$

$$v_{q,j,t} = v_{q,j,t} - \frac{v_{q,j,t-h}}{n_{j,t-h}} R_{i,j,t}, \quad \text{for each } i = 1, N_C; j = i, N_C. \tag{46}$$

Before marching through Eqs. (45) and (46), the first term on the right side of these equations is set to $v_{q,i,t-h}$ (which is the same as $v_{q,j,t-h}$, since i and j describe the same size distribution). In these equations, the ratio $R_{i,j,t}/n_{i,t-h}$ is the volume (and number) fraction of particles in size bin i that is lost to temporarily coalescence of particles of size i, j. The product of this fraction and the initial volume concentration of component q in the bin $v_{q,j,t-h}$ is the volume concentration of component q lost to temporary coalescence of particles of size i, j. Equations (45) and (46) are positive so long as Eq. (42) has converged. Thus, ensuring convergence of Eq. (42) ensures a positive-definite scheme.

Finally, the volume concentration of component q added to each size bin $l = 1, N_C$ due to fragmentation of temporarily coalesced particles is

$$v_{q,l,t} = v_{q,l,t} + R_{i,j,t} Q_{i,j,l} \left(\frac{v_{q,i,t-h}}{n_{i,t-h}} + \frac{v_{q,j,t-h}}{n_{j,t-h}} \right), \quad \text{for each } i = 1, N_C; \; j = i, N_C, \tag{47}$$

where

$$Q_{i,j,l} = P_{i,j,l} \frac{v_i}{v_i + v_j} \tag{48}$$

is the volume fraction of coalesced drop pair i, j fragmenting into size bin l. The sum of $Q_{i,j,l}$ over all sizes $l = 1$, N_C for each i, j pair is unity.

In sum, the temporary coalescence/breakup scheme is positive definite for any time step, exactly volume- and volume concentration–conserving for all components of all particle sizes, and exactly volume-conserving of breakup fragments.

Finally, the discrete size-resolved lightning scheme of Jacobson and Streets (2009) is modified in the present scheme by considering that temporary coalescence followed by breakup and temporary coalescence followed by bounceoff both result in charge separation. Above a small-particle diameter of 0.005 cm, it is assumed that temporary coalescence results in breakup; otherwise, it results in bounceoff (section 2b). One minus Eq. (16) gives the noncoalescence (breakup plus bounceoff) efficiencies for all sizes. This efficiency is used in Eq. (6) of Jacobson and Streets (2009) to give the effective ''bounceoff kernel'' (or bounceoff kernel at small sizes and breakup kernel at large sizes as defined here), which is used in Eq. (5) of that paper to determine charge separation and the lightning flash rate.

3. Results

The coagulation/breakup scheme is analyzed here for accuracy against an analytical solution, stability at long time step and coarse size resolution, and convergence upon refinement of the time step and size grid.

First, results from the breakup scheme alone are compared with the analytical solution of Feingold et al. (1988), which assumes a constant breakup kernel B. The analytical solution is

$$n_{l,t} = \frac{n_{l,0} + \gamma N_0 (e^{\alpha t} - 1) e^{-\gamma v_l} dv_l}{1 + \frac{1}{b}(e^{\alpha t} - 1)}, \tag{49}$$

where $n_{l,t}$ is the number concentration (particles per cubic centimeter) of drops in size bin l at time t, b is a positive integer that characterizes the fragment concentration ($b = 1$ indicates no change in the summed number concentration of particles over time and $b = 2, \ldots$ represent an increase), $\gamma = bN_0/V_0$, $\alpha = bBN_0$, and N_0 and V_0 are the summed number and volume concentration ($\text{cm}^3\ \text{cm}^{-3}$) of the initial number concentration size distribution $n_{l,0}$. The summed drop number concentration as a function of time is $N_t = bN_0 e^{\alpha t}/(b + e^{\alpha t} - 1)$. The analytical solution assumes a breakup size distribution (number of fragments in size bin l due to breakup of the temporarily coalesced pair i, j) for use in Eq. (44) of the form

$$P_{i,j,l} = \gamma^2 (v_i + v_j) e^{-\gamma v_l} dv_l. \tag{50}$$

Figure 4 compares results from the model with those from the analytical solution for two cases described in the caption with a model time step of 300 s. The model results are nearly indistinguishable from those of the analytical solution in both cases and become completely indistinguishable at greater time resolution. Feingold et al. (1988) similarly show that results from their two-moment scheme follow those of the analytical solution nearly exactly, but with a time step of 3 s. Those of a one-moment scheme they tested retarded breakup slightly.

Figure 5 shows model results alone after 12 h of coagulation/breakup of an initial Marshall–Palmer size distribution (Marshall and Palmer 1948). Solutions for different size bin resolutions at the same time step (Fig. 5a) and solutions for different time steps at the same size bin resolutions (Fig. 5b) are shown. In all cases, the solutions equilibrate, as found in many previous studies that used an initial Marshall–Palmer distribution (e.g., List et al. 1987; Hu and Srivastava 1995; Brown 1999; S05). The equilibrated solutions converge upon a refinement of each the size bin resolution and the time step. All solutions conserve volume exactly, are positive definite, and are unconditionally stable (stable for any time step and size bin resolution).

Figure 6a shows results from a high-resolution (1-s time step, 300 bins) simulation of coagulation alone versus coagulation combined with breakup after 1 h of simulation, where the model was initialized with a lognormal cloud drop distribution. Results at 1 s and 300 bins are considered here to be the ''exact'' numerical solution for comparison with subsequent tests at coarser temporal and size resolution. The difference between the two curves shown indicates that treating breakup is important for ensuring that coagulated particles do not become artificially large and that a model predicts a sufficient number of particles smaller than raindrop size to simulate cloud optical depths physically. The broader size distribution that results from treating breakup is also important since the evaporation

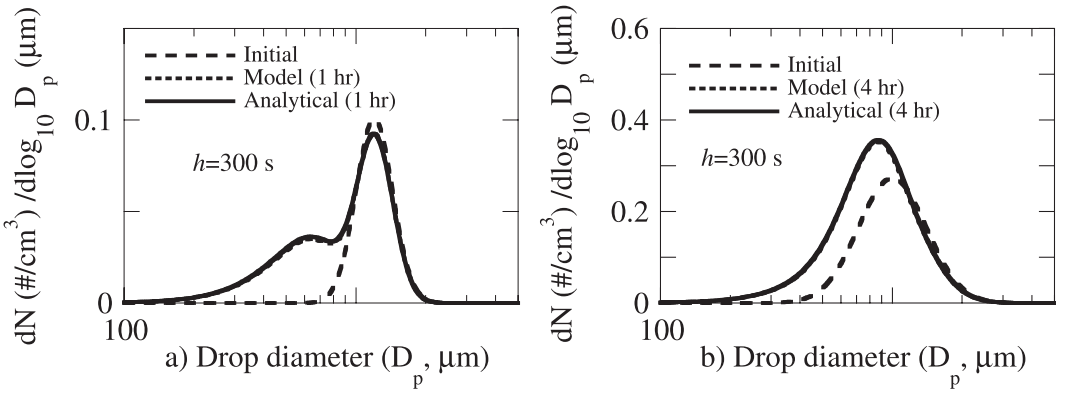

FIG. 4. Comparison of the model numerical solution to drop breakup alone with the analytical solution of Feingold et al. (1988), which assumes a constant breakup kernel B. Figures are for (a) $b = 8$, $B = 10^{-3}$ cubic centimeters per particle per second, initial geometric mean number diameter $D_g = 1200$ μm, initial geometric standard deviation $\sigma_g = 1.2$, $N_0 = 0.02$ particle per cubic centimeter, 300 size bins, a simulation time of 1 h, and a model time step of $h = 300$ s and (b) $b = 4$, $B = 10^{-4}$ cubic centimeters per particle per second, $D_g = 1000$ μm, $\sigma_g = 1.4$, $N_0 = 0.1$ particle per cubic centimeter, 300 size bins, a simulation time of 4 h, and $h = 300$ s.

rate of drops below cloud base depends significantly on particle size, with smaller particles evaporating faster. Thus, a broader distribution is likely to result in more water reevaporation below cloud base. The figure also indicates that breakup may be responsible for reproducing some drops below 4-μm diameter although this result depends highly on the accuracy of the breakup distribution parameterization used.

Figure 6b shows the result for the coagulation plus breakup case in Fig. 6a at different size bin resolutions and at a 60-s time step. The result for 300 bins and 1 s (the so-called exact solution) is also shown for comparison. The figure indicates relatively little difference in the solution at a 60-s time step and at 30 size bins relative to the exact solution, which is good news considering that the exact solution requires about 41 000 times more computer time on one processor for a 1-h simulation than that at 60 s and 30 bins (652 s versus 0.016 s on an Intel Xeon 5260, 3.33 GHz).

Figure 6c shows the result for coagulation plus breakup after 1 h at different time steps, all over 30 size bins. The figure indicates that the solutions for 1, 30, and 60 s are quite similar but those at 300, 600, and 1800 s begin to diverge. In all cases, though, the solutions are volume conservative, positive definite, and unconditionally stable.

To obtain a better idea of computer timings, some of the simulations in Fig. 6c were run for 1 yr continuously in a box model. The computer times for 60-, 300-, and 600-s time steps were 98.2, 23.6, and 12.4 s yr^{-1}, respectively, on the single processor listed above. The times suggest

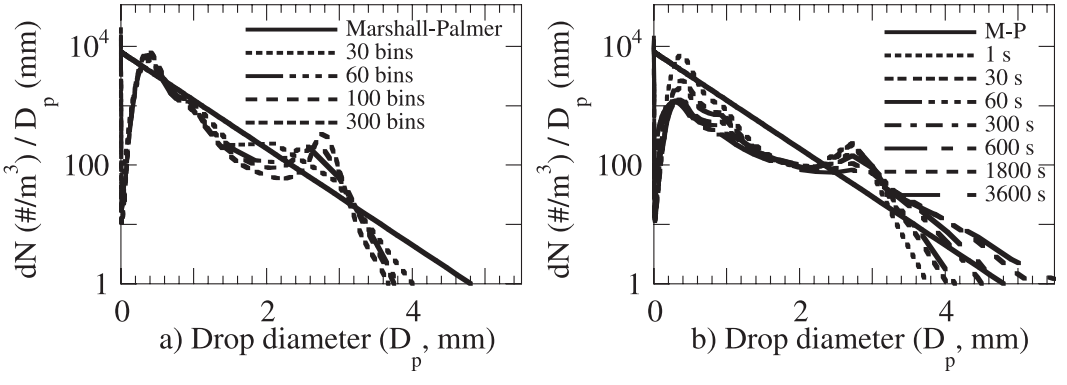

FIG. 5. Equilibrium solution (after 12 h) of collision/coalescence and breakup [all terms in Eq. (1)] resulting from an initial Marshall–Palmer size distribution, $dN/D_p = N_0 \exp(-4.1R^{-0.21}D_p)$, where $R = 42$ mm h^{-1} is the rainfall rate, $N_0 = 8000$ mm^{-1} m^{-3}, D_p is drop diameter (mm), and the rainfall liquid water content is 2 g m^{-3}. (a) Results from four model size bin resolutions: 30 bins ($V_{rat} = 2.722$), 60 bins ($V_{rat} = 1.636$), 100 bins ($V_{rat} = 1.341$), and 300 bins ($V_{rat} = 1.102$) at $h = 1$ s. (b) Results from the same problem for four time steps at a size resolution of 100 bins. Results were obtained at a temperature of 20°C and pressure of 700 hPa.

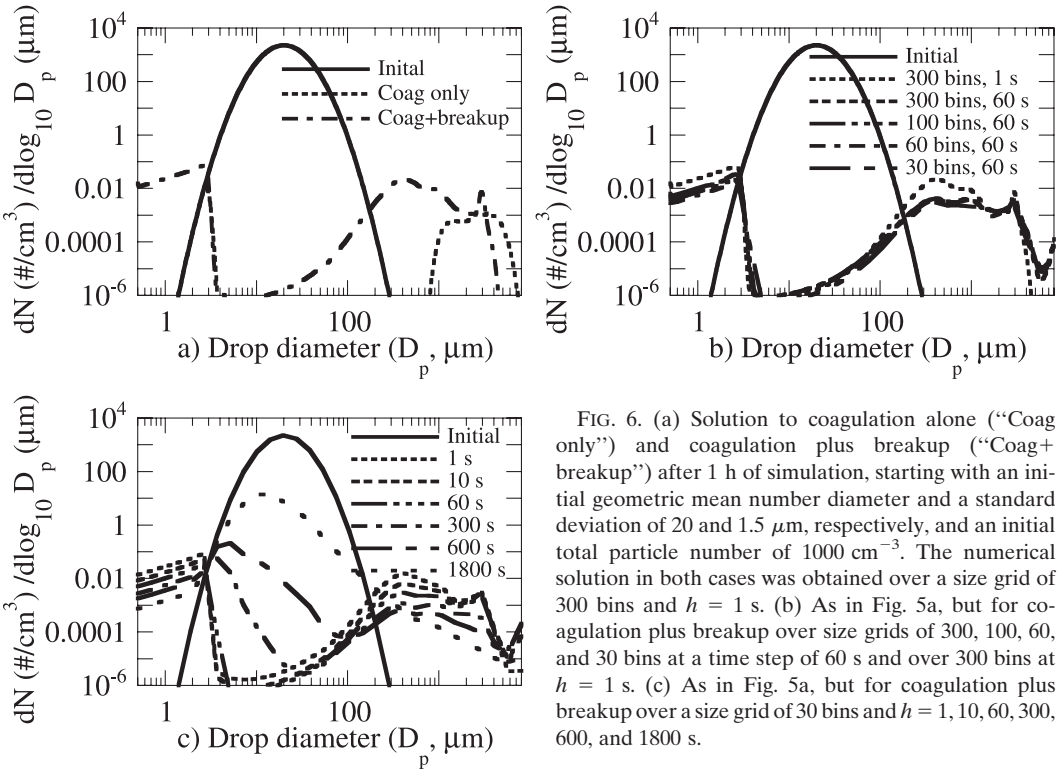

FIG. 6. (a) Solution to coagulation alone (''Coag only'') and coagulation plus breakup (''Coag+ breakup'') after 1 h of simulation, starting with an initial geometric mean number diameter and a standard deviation of 20 and 1.5 μm, respectively, and an initial total particle number of 1000 cm^{-3}. The numerical solution in both cases was obtained over a size grid of 300 bins and $h = 1$ s. (b) As in Fig. 5a, but for coagulation plus breakup over size grids of 300, 100, 60, and 30 bins at a time step of 60 s and over 300 bins at $h = 1$ s. (c) As in Fig. 5a, but for coagulation plus breakup over a size grid of 30 bins and $h = 1, 10, 60, 300, 600$, and 1800 s.

that a factor of 10 increase in the time step size resulted in about a factor of 8 decrease in computer time. A greater decrease in computer time did not occur since a few more iterations were required per time step at longer time steps to converge the breakup iteration. Coagulation (which is noniterative) required 20.2%, 17.1%, and 16.0% of the time, respectively, for each time step. Thus, breakup required about 5–6 times more computer time than did coagulation.

Timing tests in a global model

The new cloud drop breakup scheme described here was implemented into the nested Gas, Aerosol, Transport, Radiation, General Circulation, Mesoscale, and Ocean Model (GATOR-GCMOM), a global–urban climate–weather–air pollution model (Jacobson et al. 2007; Jacobson and Streets 2009; Jacobson 2010), and computer timings were obtained.

Previously, the model treated cloud collision/coalescence (coagulation) among size- and composition-resolved liquid, ice, and graupel in the same manner as described here but parameterized liquid drop breakup simply by redistributing drops larger than a certain size with a single breakup distribution, as described in Jacobson (2003). Also, the previous scheme used a longer time step for both coagulation and breakup, either 1800 or 3600 s. The scheme here is more physical as it treats breakup due to specific drop pair interactions; however, it is iterative and thus takes more computer time.

In the present application, the model was applied over ~188 000 grid cells (4° × 5° resolution in the horizontal and 58 layers in the vertical, including 14 layers above 18 km. The model treated three hydrometeor size distributions (liquid, ice, and graupel), 30 size bins per distribution, and 16 chemical component inclusions per size bin, and the particle number in each bin. Coagulation and breakup were operator split. Coagulation was solved among all three hydrometeor distributions simultaneously as in Jacobson (2003), and breakup was solved over the liquid distribution. Operator-splitting time steps between coagulation and breakup of 60, 300, and 600 s were compared. The additional model computer times required in each case compared with the previous method of coagulation/breakup (where the operator split time step was 3600 s and breakup was solved noniteratively and only for the largest drops) were 6, 1.4, and 0.75 days yr^{-1} of simulation, respectively, on 24 Intel Nehalem processor cores. To put this in context, 0.75 days yr^{-1} represents ~5.5% and 6 days yr^{-1} represents ~44% of the overall computer time of the model. Thus, while the new iterative technique consumed at least 6% more time than the previous method because of both the more frequent coagulation and breakup calls and the iterative breakup solution, it should

allow for more physically correct feedbacks among cloud variables for studies of climate response.

4. Conclusions

A new volume- and volume concentration–conserving, positive-definite, iterative numerical scheme for solving temporary drop coalescence followed by breakup was developed. The scheme was coupled with an existing volume- and volume concentration–conserving non-iterative collision/coalescence code. The breakup scheme compares nearly exactly with a constant-kernel analytical solution at a 300-s time step. The combined schemes are stable and conservative, regardless of the time step and number of size bins, and convergent with higher temporal and size resolution. Geometric size spacing with 30 bins and a time step of 60 s provide a good compromise between obtaining sufficient accuracy (relative to a much higher-resolution result) and speed when applied in a 3D model, although solutions at 600-s time step and 30 bins are still stable and conservative and take one-eighth the computer time. The combined schemes were applied to the nested GATOR-GCMOM, a global–urban climate–weather–air pollution model. Coagulation was solved over liquid, ice, and graupel distributions and breakup over the liquid distribution. Each distribution included 30 size bins and 16 chemical components per bin. Timing tests demonstrate the feasibility of the scheme in long-term global simulations.

Acknowledgments. This work was supported by U.S. Environmental Protection Agency Grant RD-83337101-O, NASA Grant NX07AN25G, the NASA High-End Computing Program, the National Science Foundation, and the Department of the Army Center at Stanford University.

REFERENCES

Beard, K. V., 1976: Terminal velocity and shape of cloud and precipitation drops aloft. *J. Atmos. Sci.,* **33,** 851–864.

——, and S. N. Grover, 1974: Numerical collision efficiencies for small raindrops colliding with micron size particles. *J. Atmos. Sci.,* **31,** 543–550.

——, and H. T. Ochs, 1995: Collisions between small precipitation drops. Part II: Formulas for coalescence, temporary coalescence, and satellites. *J. Atmos. Sci.,* **52,** 3977–3996.

Binkowski, F. S., and U. Shankar, 1995: The regional particulate matter model 1. Model description and preliminary results. *J. Geophys. Res.,* **100,** 26 191–26 209.

Bleck, R., 1970: A fast approximative method for integrating the stochastic coalescence equation. *J. Geophys. Res.,* **75,** 5165–5171.

Bott, A., 2000: A flux method for the numerical solution of the stochastic collection equation: Extension to two-dimensional particle distributions. *J. Atmos. Sci.,* **57,** 284–294.

Brown, P. S., 1997: Mass conservation considerations in analytic representation of raindrop fragment distributions. *J. Atmos. Sci.,* **54,** 1675–1687.

——, 1999: Analysis of model-produced raindrop-size distributions in the small-drop range. *J. Atmos. Sci.,* **56,** 1382–1390.

Fassi-Fihri, A., K. Suhre, and R. Rosset, 1997: Internal and external mixing in atmospheric aerosols by coagulation: Impact on the optical and hygroscopic properties of the sulphate-soot system. *Atmos. Environ.,* **31,** 1392–1402.

Feingold, G., S. Tzivion, and Z. Levin, 1988: Evolution of raindrop spectra. Part I: Solution to the stochastic collection/breakup equation using the method of moments. *J. Atmos. Sci.,* **45,** 3387–3399.

Fernandez-Diaz, J. M., C. Gonzalez-Pola Muniz, M. A. Rodriguez Brana, B. Arganza Garcia, and P. J. Garcia Nieto, 2000: A modified semi-implicit method to obtain the evolution of an aerosol by coagulation. *Atmos. Environ.,* **34,** 4301–4314.

Gelbard, F., and J. H. Seinfeld, 1978: Numerical solution of the dynamic equation for particulate systems. *J. Comput. Phys.,* **28,** 357–375.

Gillespie, J. R., and R. List, 1978: Effects of collision-induced breakup on drop size distributions in steady state rainshafts. *Pure Appl. Geophys.,* **117,** 599–626.

Hounslow, M. J., R. L. Ryall, and V. R. Marshall, 1988: A discretized population balance for nucleation, growth, and aggregation. *AIChE J.,* **34,** 1821–1832.

Hu, Z., and R. C. Srivastava, 1995: Evolution of raindrop size distribution by coalescence, breakup, and evaporation: Theory and observations. *J. Atmos. Sci.,* **52,** 1761–1783.

Jacobson, M. Z., 2002: Analysis of aerosol interactions with numerical techniques for solving coagulation, nucleation, condensation, dissolution, and reversible chemistry among multiple size distributions. *J. Geophys. Res.,* **107,** 4366, doi:10.1029/2001JD002044.

——, 2003: Development of mixed-phase clouds from multiple aerosol size distributions and the effect of the clouds on aerosol removal. *J. Geophys. Res.,* **108,** 4245, doi:10.1029/2002JD002691.

——, 2005: *Fundamentals of Atmospheric Modeling*. 2nd ed. Cambridge University Press, 813 pp.

——, 2010: Short-term effects of controlling fossil-fuel soot, biofuel soot and gases, and methane on climate, Arctic ice, and air pollution health. *J. Geophys. Res.,* **115,** D14209, doi:10.1029/2009JD013795.

——, and R. P. Turco, 1994: SMVGEAR: A sparse-matrix, vectorized gear code for atmospheric models. *Atmos. Environ.,* **28,** 273–284.

——, and D. G. Streets, 2009: The influence of future anthropogenic emissions on climate, natural emissions, and air quality. *J. Geophys. Res.,* **114,** D08118, doi:10.1029/2008JD011476.

——, R. P. Turco, E. J. Jensen, and O. B. Toon, 1994: Modeling coagulation among particles of different composition and size. *Atmos. Environ.,* **28,** 1327–1338.

——, Y. J. Kaufmann, and Y. Rudich, 2007: Examining feedbacks of aerosols to urban climate with a model that treats 3-D clouds with aerosol inclusions. *J. Geophys. Res.,* **112,** D24205, doi:10.1029/2007JD008922.

List, R., N. R. Donaldson, and R. E. Stewart, 1987: Temporal evolution of drop spectra to collisional equilibrium in steady and pulsating rain. *J. Atmos. Sci.,* **44,** 362–372.

Lister, J. D., D. J. Smit, and M. J. Hounslow, 1995: Adjustable discretized population balance for growth and aggregation. *AIChE J.,* **41,** 591–603.

Low, T. B., and R. List, 1982a: Collision, coalescence and breakup of raindrops. Part I: Experimentally established coalescence

efficiencies and fragment size distributions in breakup. *J. Atmos. Sci.,* **39,** 1591–1606.

——, and ——, 1982b: Collision, coalescence, and breakup of raindrops. Part II: Parameterization of fragment size distributions. *J. Atmos. Sci.,* **39,** 1607–1619.

Marshall, J. S., and W. M. K. Palmer, 1948: The distribution of raindrops with size. *J. Meteor.,* **5,** 165–166.

McFarquhar, G. M., 2004: A new representation of collision-induced breakup of raindrops and its implications for the shapes of raindrop size distributions. *J. Atmos. Sci.,* **61,** 777–794.

Pratsinis, S. E., 1988: Simultaneous nucleation, condensation, and coagulation in aerosol reactors. *J. Colloid Interface Sci.,* **124,** 416–427.

Sandu, A., 2002: A Newton–Cotes quadrature approach for solving the aerosol coagulation equation. *Atmos. Environ.,* **36,** 583–589.

Schlottke, J., W. Straub, K. D. Beheng, H. Gomaa, and B. Weigand, 2010: Numerical investigation of collision-induced breakup of raindrops. Part I: Methodology and dependencies on collision energy and eccentricity. *J. Atmos. Sci.,* **67,** 557–575.

Seifert, A., A. Khain, U. Blahak, and K. D. Beheng, 2005: Possible effects of collisional breakup on mixed-phase deep convection simulated by a spectral (bin) cloud model. *J. Atmos. Sci.,* **62,** 1917–1931.

Straub, W., K. D. Beheng, A. Seifert, J. Schlottke, and B. Weigand, 2010: Numerical investigation of collision-induced breakup of raindrops. Part II: Parameterizations of coalescence efficiencies and fragment size distributions. *J. Atmos. Sci.,* **67,** 576–588.

Strom, J., K. Okada, and J. Heintzenberg, 1992: On the state of mixing of particles due to Brownian coagulation. *J. Aerosol Sci.,* **23,** 467–480.

Suck, S. H., and J. R. Brock, 1979: Evolution of atmospheric aerosol particle size distributions via Brownian coagulation numerical simulation. *J. Aerosol Sci.,* **10,** 581–590.

Trautmann, T., and C. Wanner, 1999: A fast and efficient modified sectional method for simulating multicomponent collisional kinetics. *Atmos. Environ.,* **33,** 1631–1640.

Tzivion, S., G. Feingold, and Z. Levin, 1987: An efficient numerical solution to the stochastic collection equation. *J. Atmos. Sci.,* **44,** 3139–3149.